Short Communication

Facile Synthesis of Hierarchical MnO@C Nanoplates for High-Performance Lithium-Ion Batteries

Chaochun Yuan[1], Kun Wang[1], Huanhuan Li[1], Yaping Wang[2,*] , Long Chen[1], Haobing Jiang[1],

[1] Automotive Engineering Research Institute, Jiangsu University, Zhenjiang 212013, P. R. China.
[2] School of Material Science & Engineering, Jiangsu University, Zhenjiang 212013, P. R. China.
[*]E-mail: wangyaping@ujs.edu.cn

A facile strategy for synthesis of hierarchical MnO@C nanoplates has been developed *via* one-step pyrolysis of Mn-glycolate coordination polymers. Core-shell MnO@C nanoparticles with ultrasmall sizes as the primary building blocks are interconnected to construct porous nanoplates. The unique architecture is favorable for the fast diffusion of lithium ions and electrons, accommodating the volume change of MnO during the lithiation/delithiation process and alleviating the side reactions on the interface between MnO and electrolyte. As a result, these hierarchical MnO@C nanoplates exhibit fascinating Li$^+$ storage performance such as high reversible capacities, good cycling stability and rate capability when served as an anode material for lithium-ion batteries.

1. INTRODUCTION

Exploring electrode materials with high energy and power density, long lifespan in lithium-ion batteries (LIBs) is crucial for their expanding applications in electrical and hybrid electrical vehicles. In this aspect, 3d transition metal oxides (TMOs) are promising anode materials for their higher theoretical capacities [1-4]. Especically, MnO has attracted considerable interests because of its high theoretical capacity (756 mAh g^{-1}), relatively low electromotive force value (1.032V vs. Li$^+$/Li), natural abundance and environmental benignity [4-6]. However, the large volume expansion/contraction of MnO during Li$^+$ insertion/extraction results in capacity fading and poor cycling life [4-6]. Integration of nanostructured MnO with conductive carbon materials not only facilitate electron and lithium-ion transport but also provide flexible space to buffer the mechanical strain of Li$^+$ insertion/extraction [5-7]. However, artificially constructing an ideal MnO/carbon nanostructure is still a challenging task.

Coordination polymers (CPs), a kind of supramolecular compounds formed by multidentate organic ligands and metal ions, are attractive for their intriguing structures and applications [8]. Because of the richness of the ligands and secondary building units, the structures and morphologies of CPs are always various and controllable [9-11]. Moreover, transition metals and carbon containing groups (organic ligands) with ordered and repeated arrangement are simultaneously contained in a CP. Thus, employing CPs as sacrificial precursors for preparing TMO/carbon nanocomposites is feasible [12-14]. However, facile synthesis of TMO/carbon nanocomposites from CPs is an ongoing research focus.

Here, a green and facile route is successfully developed for fabricating hierarchical MnO@C nanoplates assembled by core-shell MnO@C nanoparticles from pyrolysis of Mn-glycolate coordination polymers. The unique architecture exhibits fascinating electrochemical performance, such as high reversible capacity, excellent cycling stability and good rate capability, when evaluated as an anode material for LIBs.

2. EXPERIMENTAL

In a typical synthesis, 1.5 g $Mn(CH_3COO)_2 \cdot 4H_2O$ (J&K, 98%) was dissolved in 50 ml ethylene glycol (J&K, 99.5%) under vigorous stirring to get a transparent solution. Then, the solution was maintained at 170 °C with refluxing for 2 h in an oil bath. After cooling, the white precipitates (Mn-glycolate CPs) were filtered, washed with ethanol, and dried at 80 °C for 6 h. To obtained hierarchical MnO@C nanoplates, the precursor was calcined in Ar (99.999%) at 500 °C for 2h with a ramp of 2 °C min^{-1}.

The phases of the obtained products were collected on a Bruker D8 Advance X-ray diffractometer (Cu Kα radiation, $\lambda = 0.15406$ Å). The morphologies were examined by field-emission scanning electron microscopy (SEM, FEI Nova NanoSEM450) and transmission electron microscope (TEM, JEOL, JEM-2100HR). Carbon content in hierarchical MnO@C nanoplates was obtained on a Perkin-Elmer 240C elemental analyzer.

The electrochemical performance of hierarchical MnO@C nanoplates was investigated using coin-type cells (CR2032) assembled in an argon-filled glove box. The test electrodes were made from the mixture of active material, super p li, and polyvinylidene fluoride (PVDF) binder at a weight ratio of 70:20:10. The electrolyte was 1 mol/L $LiPF_6$ in ethylene carbonate (EC)/diethyl carbonate (DEC) (1:1, v/v). Lithium foil was used as counter electrode. Charge/discharge tests were performed between 0.01 and 3.0 V (vs. Li^+/Li) on a Land CT2001C battery tester.

3. RESULTS AND DISCUSSION

Fig. 1a shows the XRD pattern of the obtained precursor. It is the typical products from polyol-mediated processes for the strong peak at around 10°, which should be ascribed to the formation of Mn-glycolate coordination polymers in our synthesis [15,16]. The morphologies of the precursor are elucidated *via* SEM and TEM images, as shown in Fig. 1b, 1c and 1d. Large quantities of platelike

nanostructures are clearly observed in Fig. 1b. The average diameter is about 5 μm, as can be seen in Fig. 1c. A magnified view in Fig. 1d represents that the nanoplate has a smooth surface.
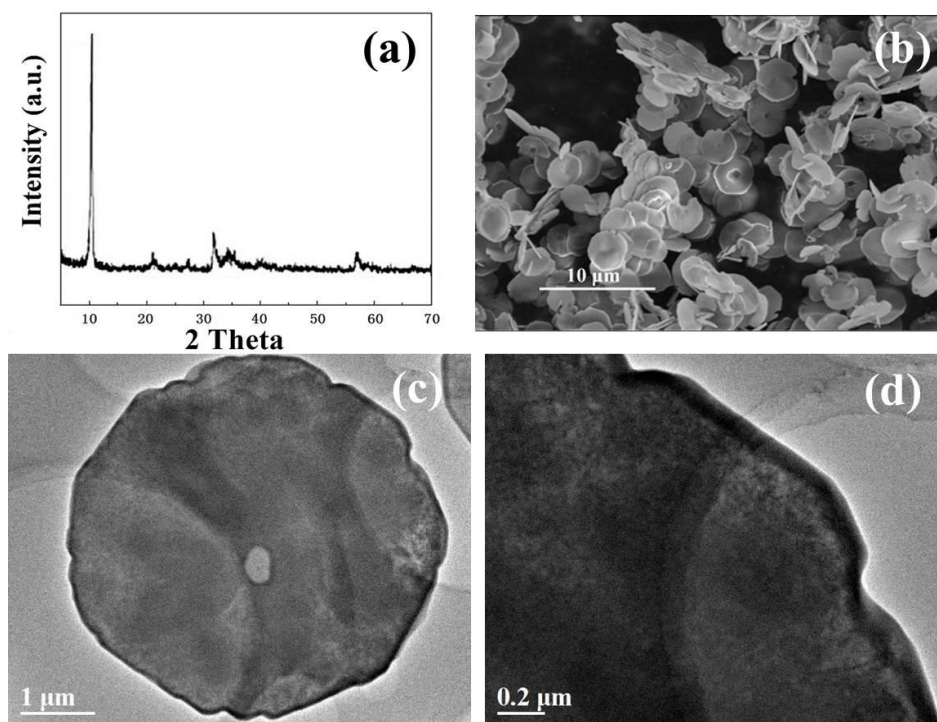
Figure 1. XRD pattern (a), SEM (b) and TEM (c,d) images of Mn-glycolate precursor.

Fig. 2a shows the XRD pattern of the obtained MnO@C nanocomposite. All peaks can be indexed to the cubic structure of MnO with a space group *Fm-3m* (JCPDS card no. 89-4853). No diffraction peaks of crystalline carbon (graphite) are observed. However, a carbon content of 15.7 wt% can be detected in the sample through elemental analysis. Thus, the carbon in the sample should be amorphous. In view of the above, it is concluded that Mn-glycolate precursor is successfully transformed to MnO@C nanocomposite.

SEM images of as-prepared MnO@C are illustrated in Fig. 2b and c. The calcined product well inherits the morphology of Mn-glycolate precursor at first glance (Fig. 2b). In the enlarge view, the MnO@C nanoplates show hierarchical nanostructures with plenty of ordered nanopores (Fig. 2c). In the TEM images (Fig. 2d and e), it is obvious that the MnO@C nanoplates are highly porous and made up of interconnected nanosized subunits. The subunits have a core-shell structure with ultrasmall sizes (about 7 nm in diameter), as illustrated in HRTEM image (Fig. 2f). The interplanar spacing between lattice fringes in the core is 0.222 nm, which can be attributed to the (200) plane of MnO. Moreover, the shell has an amorphous feature without lattice fringes, which could be ascribed to amorphous carbon.
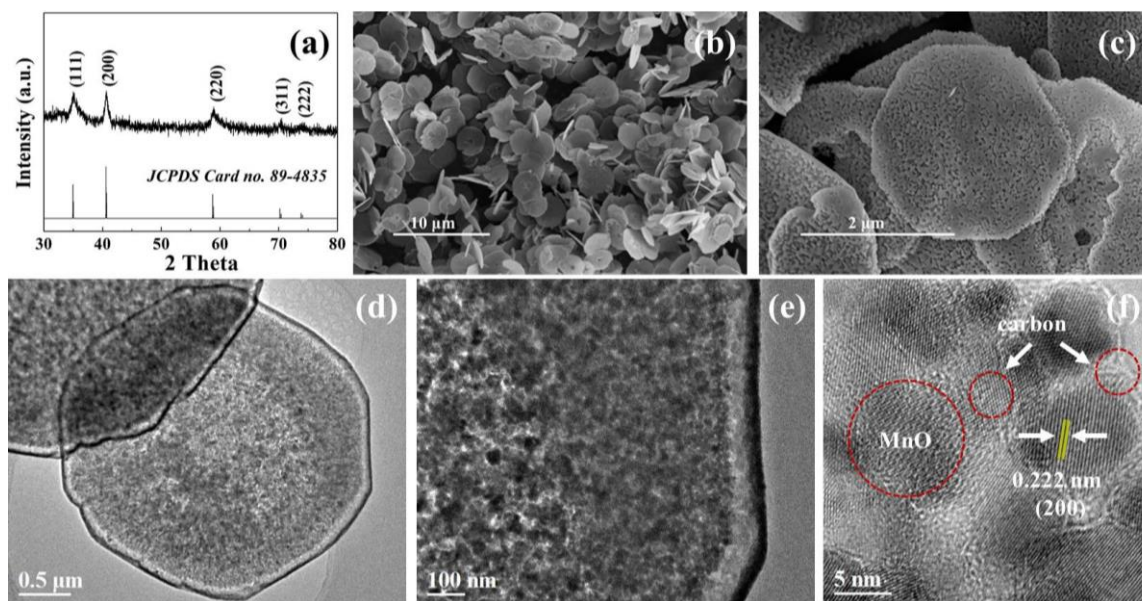
Figure 2. (a) XRD pattern of hierarchical MnO@C nanoplates. Vertical bars below the pattern show the positions of all possible reflection peaks. The hkl labels are placed according to the reflection position. (b,c) SEM images of hierarchical MnO@C nanoplates. (d,e) TEM and (f) HRTEM images of hierarchical MnO@C nanoplates.

Fig. 3a shows the cycling performance of hierarchical MnO@C nanoplates at a current density of 100 mA g^{-1}. In the first cycle, the discharge capacity is 1847 mAh g^{-1}, while the relative charge capacity is 1170 mAh g^{-1}, leading to a coulombic efficiency of around 63%. Then, the capacities gradually decrease during cycling. After thirty cycles, hierarchical MnO@C nanoplate electrode is higly reversible with charge and discharge capacities of 800 and 830 mAh g^{-1}, respectively. Moreover, the coulombic efficiency remains at about 96%, suggesting an excellent reversible Li^{+} intercalation/extraction associated with efficient transport of electrons.

Fig. 3b shows the galvanostatic charge/discharge curves of the first three cycles for hierarchical MnO@C nanoplates at 100 mA g^{-1}. In the initial discharge, the discharge voltage plateau at about 0.4 V is different from those of other cycles at about 0.5 V, indicating the irreversible reactions including the inevitable formation of SEI and decomposition of electrolyte in the first discharge, which are common for MnO anode materials [4-7]. Moreover, the charge voltage plateau is kept at about 1.2 V in the first three cycles. No obvious change of voltage plateau in both charge and discharge profiles is observed beyond the first cycle, showing excellent electrochemical reversibility.

Motivated by the excellent cyclic performance of hierarchical MnO@C nanoplates, rate capability is also evaluated at various current densities from 0.1 to 1 A g^{-1}. As shown in Fig. 3c, the discharge capacities of 830, 670 and 550 mAh g^{-1} can be obtained at current densities of 200, 500 and 800 mA g^{-1}, respectively. Even at a high rate of 1 A g^{-1}, the reversible discharge capacity of 420 mAh g^{-1} can be observed, which is still higher than the theoretical capacity of graphite (372 mAh g^{-1}). When the current density returns to 0.1 A g^{-1}, the discharge capacity is recovered to 1000 mAh g^{-1}, also indicating the good reversibility of hierarchical MnO@C nanoplates.
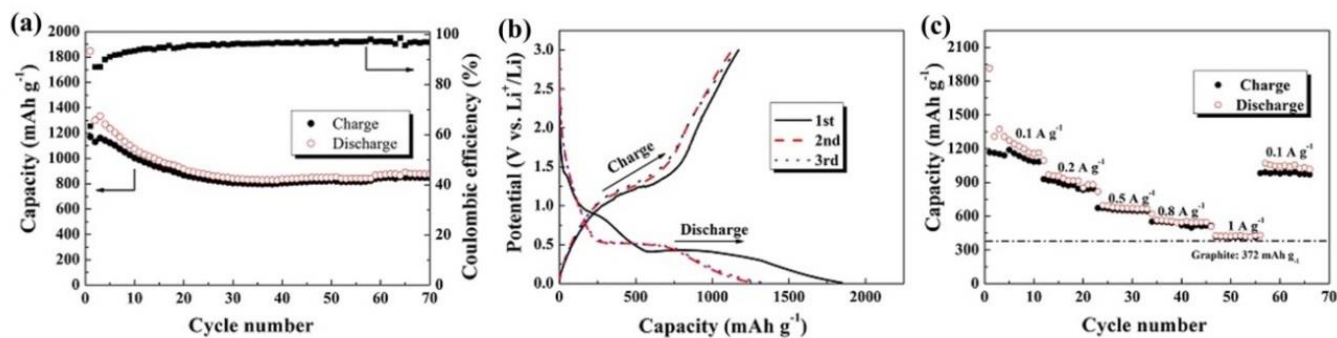
Figure 3. (a) Cyclic performance of hierarchical MnO@C nanoplates at 100 mA g^{-1}. (b) The discharge/charge curves of the first three cycles for hierarchical MnO@C nanoplates at a current rate of 100 mA g^{-1} between 0.01 and 3.00 V. (c) Cyclic performance of hierarchical MnO@C nanoplates at different current densities.

Table 1 Comparison of electrochemical performance of hierarchical MnO@C nanoplates with those MnO/C composite anodes reported.

Sample	Cycling performance	Rate capability
This work	830 mAh g^{-1} after 70 cycles	550 mAh g^{-1} at 0.8 A g^{-1}
Porous MnO/C [17]	861.3 mAh g^{-1} after 130 cycles	511.7 mAh g^{-1} at 0.8 A g^{-1}
Cross-linked MnO@C [18]	615 mAh g^{-1} after 100 cycles	497.4 mAh g^{-1} at 0.5 A g^{-1}
Biotemplated MnO/C microtubes [19]	610 mAh g^{-1} after 60 cycles	462 mAh g^{-1} at 1 A g^{-1}
MnO/C microsheets [20]	797.6 mAh g^{-1} after 50 cycles	429.4 mAh g^{-1} at 0.8 A g^{-1}
MnO/C composites [21]	740 mAh g^{-1} after 50 cycles	565 mAh g^{-1} at 1 A g^{-1}
MnO/C core-shell nanowires [22]	903 mAh g^{-1} after 60 cycles	610 mAh g^{-1} at 1 A g^{-1}
MnO multi-core@nitrogen-doped carbon shell nanoparticles [23]	578 mAh g^{-1} after 60 cycles	254 mAh g^{-1} at 1 A g^{-1}

According to these experimental facts, hierarchical MnO@C nanoplates derived from Mn-glycolate precursor displays excellent Li$^+$ storage performance. These properties are competitive as compared with the previous reports on MnO/C anode materials (Table 1) [17-23]. They might be assigned to the combination of the benefits in the structure and components of the hierarchical MnO@C nanoplates, which relieve the volume effect during Li$^+$ insertion/extraction, alleviate the side reactions on the interface between electrode and electrolyte, and maintain an efficient and continuous electrical connectivity.

4. CONCLUSIONS

In conclusion, a facile approach was developed for fabrication of hierarchical MnO@C nanoplates. This unique nanoarchitecture combines the superior properties of porous structure, ultrafine core-shell structured MnO@C subunit, and conductive elastic buffering framework. The electrodes made of these hierarchical MnO@C nanoplates exhibit excellent Li$^+$ storage performance such as high reversible capacity, excellent cycling stability and rate capability. The present approach is

not only convenient but also cost-effective, and therefore is promising for the fabrication of other metal oxide/carbon nanocomposites with well-defined structures.

References

1. L. Zhang, H. B. Wu, S. Madhavi, H. H. Hng and X. W. Lou, *J. Am. Chem. Soc.*, 134 (2012) 17388.
2. K. Z. Cao, L. F. Jiao, Y. C. Liu, H. Q. Liu, Y. J. Wang and H. T. Yuan, *Adv. Funct. Mater.*, 25 (2015) 1082.
3. S. Mohapatra, S. V. Nair, D. Santhanagopalan and Rai A. K., *Electrochim. Acta*, 206 (2016) 217.
4. X. Y. Fan, S. H. Li and L. Lu, *Electrochim. Acta*, 200 (2016) 152.
5. Y. Xia, Z. Xiao, X. Dou, H. Huang, X. H. Lu, R. J. Yan, Y. P. Gan, W. J. Zhu, J. P. Tu, W. K. Zhang and X.Y. Tao, *ACS nano*, 7 (2013) 7083.
6. X. Zhang, Z. Xing, L. L. Wang, Y. C. Zhu, Q. W. Li, J. W. Liang, Y. Yu, T. Huang, K. B. Tang, Y. T. Qian and X. Y. Shen, *J. Mater. Chem.*, 22 (2012) 17864.
7. S. J. Ma, D. M. Chen and W. L. Wang, *Phys. Chem. Chem. Phys.*, 18 (2016) 19130.
8. O. K. Farha and J. T. Hupp, *Acc. Chem. Res.*, 43 (2010) 1166.
9. Y. Z. Fan, R. M. Liu, W. Du, Q. Y. Lu, H. Pang and F. Gao, *J. Mater. Chem.*, 22 (2012) 12609.
10. C. C. Li, L. Mei, L. B. Chen, Q. H. Li and T. H. Wang, *J. Mater. Chem.*, 22 (2012) 4982.
11. M. H. Pham, T. Vuong, A. T. Vu and T. O. Do, *Langmuir*, 27 (201) 15261.
12. W. J. Meng, W. Chen, L. Zhao, Y. Huang, M. S. Zhu, Y. Huang, Y. Q. Fu, F. X. Geng, J. Yu, X. F. Chen and C. Y. Zhi, *Nano Energy*, 8 (2014) 133.
13. S. H. Wang, M. Q. Chen, Y. Y. Xie, Y. N. Fan, D. W. Wang, J. J. Jiang, Y. G. Li, H. Grützmacher and C. Y. Su, *Small*, 12 (2016) 2365.
14. H. H. Li, R. Y. Xu, Y. P. Wang, B. B. Qian, H. B. Wang, L. Chen, H. B. Jiang, Y. L. Yang and Y. Y. Xu, *RSC Adv.*, 4 (2014) 51960.
15. Y. F. Deng, Z. E. Li, Z. C. Shi, H. Xu, F. Peng and G. H. Chen, *RSC Adv.*, 2 (2012) 4645.
16. L. Chang, L. Q. Mai, X. Xu, Q. Y. An, Y. L. Zhao, D. D. Wang and X. Feng, *RSC Adv.*, 3 (2013) 1947.
17. Y. F. Xu, G. L. Xu, H. Su, Y. Chen, J. C. Fang, Q. Wang, L. Huang, J. T. Li and S. G. Sun, *J. Alloys Compd.*, 676 (2016) 156.
18. X. Y. Zhou, T. Bai, J. Yang, K. Wen and C. W. Liu, *Ionics*, 22 (2016) 779.
19. J. F. Wang, W. Liu, J. X. Chen, H. L. Wang, S. Liu and S. G. Chen, *Electrochim. Acta*, 188 (2016) 210.
20. J. L. Liu, N. Chen and Q. M. Pan, *J. Power Sources*, 299 (2015) 265.
21. W. J. Zhu, H. Huang, W. K. Zhang, X. Y. Tao, Y. P. Gan, Y. Xia, H. Yang and X. Z. Guo, *Electrochim. Acta*, 152 (2015) 286.
22. C. B. Zhang, J. G. Wang, D. D. Jin, K. Y. Xie and B. Q. Wei, *Electrochim. Acta*, 180 (2015) 990.
23. H. Liu, Z. H. Li, Y. R. Liang, R. W. Fu and D. C. Wu, *Carbon*, 84 (2015) 419.